 FDMP, vol.7, no.4, pp.329-340, 2011

A Computational Study of High-Speed Droplet Impact

T. Sanada[1], **K. Ando**[2] **and T. Colonius**[2]

Abstract: When a droplet impacts a solid surface at high speed, the contact periphery expands very quickly and liquid compressibility plays an important role in the initial dynamics and the formation of lateral jets. The high speed impact results in high pressures that can account for the surface erosion. In this study, we numerically investigated a high speed droplet impacts on a solid wall. The multicomponent Euler equations with the stiffened equation of state are computed using a FV-WENO scheme with an HLLC Riemann solver that accurately captures shocks and interfaces. In order to compare the available theories and experiments, 1D, 2D and axisymmetric solutions are obtained. The generated pressures, shock speeds, and differences in the dimensionality are investigated. In addition, the effect of target compliance is evaluated.

Keywords: numerical simulation, high-speed, droplet, target compliance.

1 Introduction

When a high speed droplet impacts on a solid wall, there is an important initial stage (Lesser and Field (1983)) during which the curved liquid surface is compressed and non uniform pressure distribution is generated. This initial stage creates high pressure which is greater than the well-known water hammer pressure(Cook (1928)),

$$P = \rho_l C_l V_i \tag{1}$$

where p is the generated pressure, ρ_l is the liquid density, C_l is the sonic speed of the liquid, V_i is the impact speed. The high speed impact can generate high pressure of order GPa, so that the target material is often damaged because the pressure is large enough compared to the yield stress. However, the several models for predicting this pressure have been proposed from theoretical, experimental and numerical studies. The generalized form of the water hammer relation Eq. (1) that

[1] Shizuoka University, Hamamatsu, Shizuoka, Japan.
[2] California Institute of Technology, Pasadena, CA, USA.

accounts for the target compressibility (Gardner (1932) and de Haller (1933), see Brunton and Rochester (1979)) can be written as

$$P = \frac{\rho_l C_l \rho_s C_s V_i}{\rho_l C_l + \rho_s C_s} = \frac{\rho_l C_l V_i}{1+\bar{Y}} \tag{2}$$

where the subscripts s and l denote solid and liquid, respectively, $\bar{Y}$ is the target compliance defined as the ratio of acoustic impedance between solid and water (liquid droplets). Small values $\bar{Y}$ of correspond to stiff material. These 1-dimensional linear theories Eq. (1) and Eq. (2) may be extended to large Mach number cases using relationship between shock wave velocity and liquid particle velocity (Heymann (1968); Huang, Hammitt, and Mitchell (1973)).

During the impact of cylindrical or spherical droplets, the dimensionality plays a role to generate complex pressure distributions. Heymann (1969), Lesser (1981) and Field, Lesser, and Dear (1985) theoretically estimated that the droplet center pressure can be predicted by the water hammer pressure Eq. (1) but the deformed edge pressure can reach 3 times higher than the water hammer pressure. They also argued that the pressure inside the cylindrical droplet is higher than in the spherical case, but edge pressure is identical for both cases (Lesser (1981), Field, Lesser, and Dear (1985)). The experiment of Rochester and Brunton (1979) agrees with their argument, but some experiments show discrepancy. For example, Engel (1955, see Brunton (1966)) proposed modified water hammer pressure as,

$$P = 1/2\alpha\rho_l C_l V_i \tag{3}$$

where α approaches unity for high impact velocities and the factor of 1/2 is a consequence of the spherical shape of droplet.

In this study, we simulate a high speed droplet impact on a solid wall and focus on the generated pressure. Although Haller, Ventikos, Poulikakos, and Monkewitz (2002) have numerically investigated a droplet impact in detail but they especially focused on jetting time. In addition they have only solved the one case $V_i = 500$ m/s into idealized rigid surface. We change the parameters of the stiffened equation of state and examine the effect of target compliance on this generated pressure due to the droplet impact.

2 Numerical method

With neglect of surface tension and any diffusions, the flow is govern by the Euler equations (conservation form):

$$\frac{\partial \boldsymbol{q}}{\partial t} + \nabla \cdot \boldsymbol{f}(\boldsymbol{q}) = 0, \qquad \boldsymbol{q}(\boldsymbol{x},t) = \begin{pmatrix} \rho \\ \rho \boldsymbol{u} \\ E \end{pmatrix}, \qquad \boldsymbol{f}(\boldsymbol{q}) = \begin{pmatrix} \rho \boldsymbol{u} \\ \rho \boldsymbol{u}\boldsymbol{u} + p\boldsymbol{I} \\ (E+p)\boldsymbol{u} \end{pmatrix} \tag{4}$$

where $\boldsymbol{u}$ is the velocity vector, E is the total energy and $\boldsymbol{I}$ is the identity tensor. Flows in one and two dimensions (with and without azimuthal symmetry) are considered. In order to close the Euler equations, we employed the stiffened equation of state (Harlow and Amsden (1971)),

$$\frac{p}{\gamma-1}+\frac{\gamma P_\infty}{\gamma-1}=E-\rho\boldsymbol{u}\cdot\boldsymbol{u} \tag{5}$$

where P_∞ is the stiffness constant and $P_\infty=0$ for gases. For gases, γ is the ratio of specific heats. For water, γ is a constant similar to the exponent of density in the Tait equation of state. In this study we simulate a high pressure due to high speed droplet impact. Such high pressure condition, more specifically at pressure which are large compare to the yield stress, solid substance behave essentially as compressible fluids (Thompson (1988)); hence even the solid dynamics may be described by the constitutive equation for the fluids. γ and P_∞ were chosen from the literature. In the preliminary calculation test problem, we used those from Chen and Liang (2008). For the droplet impact problem we took those from Saurel and Abgrall (1999) and Haller, Ventikos, Poulikakos, and Monkewitz (2002) . The parameters used are summarized in Tab. 1 and Tab. 2.

A third-order WENO scheme with an HLLC Riemann solver (Johnsen and Colonius (2006)) that accurately captures shocks and interfaces was used to solve the system. A third-order TVD Runge-Kutta scheme (Shu and Osher (1988), Gottlieb and Shu (1998)) was employed to march the equations forward in time. Note that this method has been shown to accurately resolve shock-bubble interaction problems (Johnsen and Colonius (2009)).

Table 1: Stiffened EOS parameters for preliminary test

Phase	$\rho[\mathrm{kg/m^3}]$	$p[10^5\mathrm{Pa}]$	γ	$P_\infty[10^9\mathrm{Pa}]$
Air (at rest)	1.2	1	1.4	0
Air (behind shock wave)	2.212	2.354	1.4	0
Water[1]	1000	1	1.392	1.1645

The computational domain is shown in Fig. 1. Fig. 1 (a) shows the preliminary test case. In this calculation, the condition was set to be same as that of Chen and Liang (2008). This condition is corresponding to the experiment of Igra and Takayama (1999, 2001). The Mach number for the incident planar shock wave was 1.47. A

[1] Chen and Liang (2008)
[2] Saurel and Abgrall (1999)
[3] Haller, Ventikos, Poulikakos, and Monkewitz (2002)

Table 2: Stiffened EOS and target compliance parameters for droplet impact problems

Phase	$\rho[\mathrm{kg/m^3}]$	γ	$P_\infty[10^9\mathrm{Pa}]$	$C[\mathrm{m/s}]$	$\bar{Y}$
Uranium / Rhodium[2]	17204	3.53	36.6	2740	0.04
Epoxy / Spinel[2]	2171	3.47	5.98	3090	0.26
Water[3]	1000	4.4	0.613	1750	1.00

uniform grid with 800×800 points was used. Fig. 1 (b) shows the schematic of droplet impact problems. In this simulation, we consider a moving solid material that impacts a stationary droplet. This replicates the experiment of Camus (1971). Hence in the computational domain, there are a droplet, a shock front in air and a solid component, and the solid impact to the droplet with the particle (piston) velocity of the shock wave. Uniform grids of 1000 points, 1500×750 points were used for 1D, 2D and axisymmetric cases, respectively. Non-reflecting boundary conditions are implemented at boundaries.

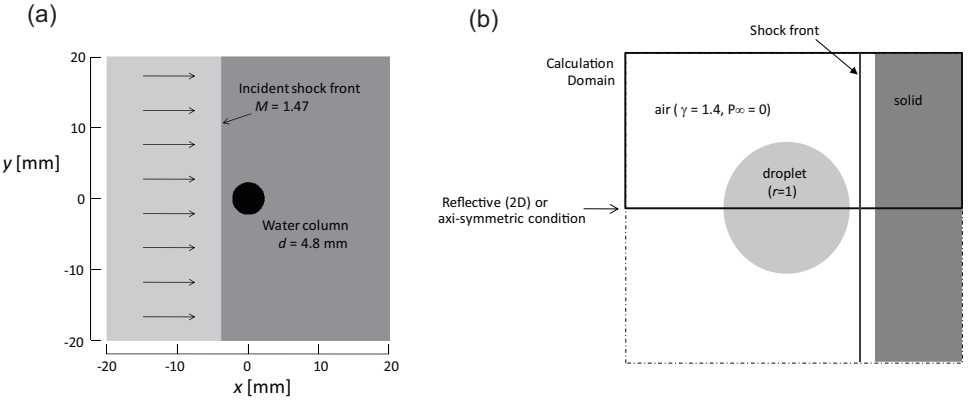

Figure 1: Schematic of calculation domain, (a) preliminary test (droplet - shock interaction), (b) droplet impact problem

Key calculation parameters are impact Mach number M_i and Target compliance $\bar{Y}$. M_i is defined as the ratio of the impact velocity to the sonic speed of the liquid

$$M_i = \frac{V_i}{C_l}. \tag{6}$$

M_i varies from 0.05 to 1.0. $\bar{Y}$ changes 0.04, 0.26 and 1.0. Note that $\bar{Y}$ of 0.04 can be regarded as an effectively rigid target (Field, Dear, and Ogren (1989)).

3 Results and Discussion

3.1 preliminary test

First we solve the shock droplet interaction problem as a preliminary test. Fig. 2 shows the sequence of the shock/droplet interaction. First (Fig. 2(b)), the incident shock wave hits the water column and the reflected shock wave (RW) generates. The transmitted wave (TW) appears inside the water column. As pointed out by Chen and Liang (2008) only a few percent of the energy is transmitted as a compression wave due to the acoustic impedance difference. The transmitted wave propagates faster than the incident shock wave, because the sonic speed of water is greater than that of air. The compression wave inside the water column reflects at the interface as an expansion wave and focuses due to the curved surface. This creates a local low-pressure (LLP) region as shown in Fig. 2. The focused expansion wave propagates upstream and reflects as a compression wave at the interface. Then a local high-pressure (LHP) region appears (Fig. 2). Inside the liquid column, these wave reflections are repeated. After the incident shock wave passes the water column, diffracted shock waves (DW) are observed (Fig. 2 (d)) and a vortex pair (VP) is generated (Fig. 2 (e)). This is similar to the case of shock wave passing through a convex corner. These results quantitatively agree with the numerical analysis by Chen and Liang (2008) and the experiment by Igra and Takayama (1999, 2001).

3.2 droplet impact problem

Next, we discuss the problem of droplet impact on a solid wall. One-dimensional Riemann problem that may replicate the initial stage of a droplet impact on a solid wall is first considered. Initially both liquid and solid phases are assumed to be in contact, but at the calculation start, the solid wall is set in motion toward the stationary liquid. The generated pressure and shock speed in water are plotted Fig. 3 and Fig. 4, respectively. We have changed the impact Mach number M_i from 0.05 to 1. Target compliance $\bar{Y}$ takes 0.04, 0.26 and 1. The case of $\bar{Y} = 1$ corresponds to the same acoustic impedance, i.e. the case of high speed water impacts water. The pressure is normalized by water hammer pressure Eq. (1). The figure also plots the theoretical estimation by Heymann (1968)

$$P = \rho_l C_l V (1 + k\frac{V}{C_l}). \tag{7}$$

Here, V is the particle velocity; k is the parameter that takes around 2 for water. This theory assumes that a droplet impacts a rigid target and contains the first-order

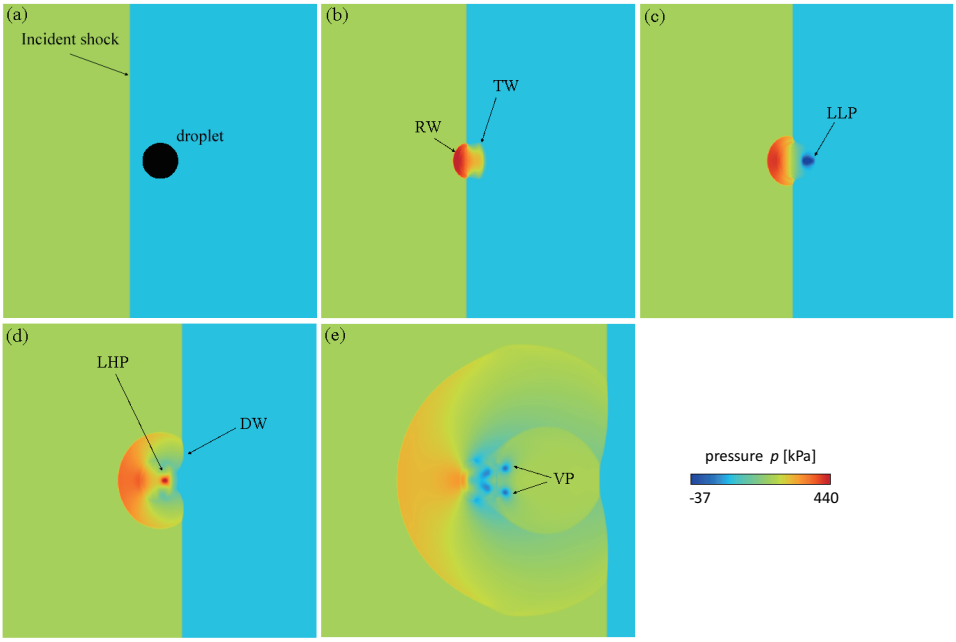

Figure 2: The pressure contours for shock interaction with water column at (a) $t = 0\mu$s, (b) $t = 4.7\mu$s, (c) $t = 6.7\mu$s, (d) $t = 13.5\mu$s, (e) $t = 40.5\mu$s. The Mach number for the incident planar shock wave is $M = 1.47$, the diameter of the water column is 4.8 mm. This computation condition is same as Igra and Takayama (1999, 2001) and Chen and Liang (2008)

correction of the shock wave velocity (Huang, Hammitt, and Mitchell (1973)). The dashed lines show the estimation from Eq. (2).

It follows from Fig. 3 that the generated pressure increases with impact Mach number M_i. For the case of $\bar{Y} = 0.04$, the generated pressure is larger than the water hammer pressure with rigid targets over a wide range of M_i. The difference in the generated pressure caused by the target compliance increases with M_i. For the case of $\bar{Y} = 1.0$, the pressure has only water hammer pressure of rigid target around $M_i = 1$. At the low M_i, the pressure approaches to the Eq. (2). Fig. 4 suggest that the linear theory which assumes the propagation speed of linear waves is invalid in this range of M_i.

Next we discuss two-dimensional and axisymmetric solutions. Fig. 5 shows the density counters of time evolution of two-dimensional droplet impact. The impact Mach number M_i is 0.2, the target compliance $\bar{Y}$ is 0.04. After the droplet impact, the droplet is deformed and a shock wave (S) is generated (Fig. 5 (b)). The shock

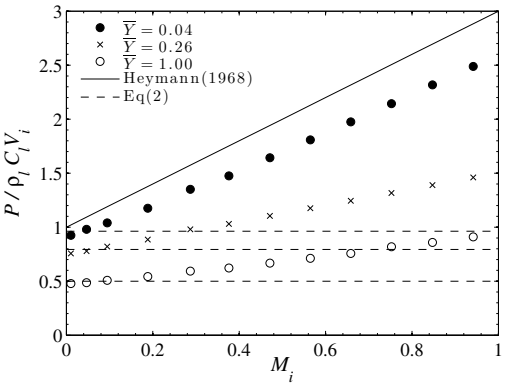

Figure 3: Generated pressure inside water in the 1D problem as a function of M_i and $\bar{Y}$

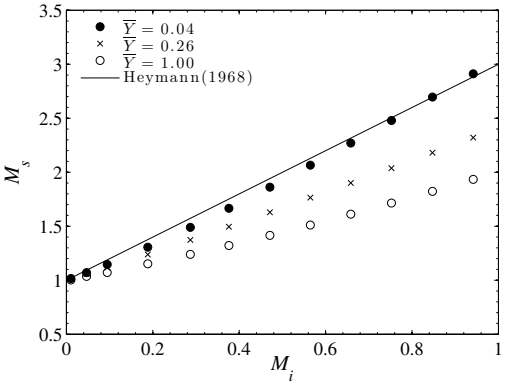

Figure 4: Generated shock speed inside water in the 1D problem

wave propagates upward and is followed by a expansion wave that appears along with the free surface (Fig. 5 (c) (d)). This low pressure region appears due to the reflection (R) of the shock wave. This is because the mismatch in acoustic impedance between air and water, and horizontal velocity components of shock wave (Haller et al. 2003). Finally the expansion wave focuses (F) at the top of droplet (Fig. 5 (e)). Also at the bottom of the droplet, side jet formation is observed (Fig. 5 (f)). The results are in qualitative agreement with the experiments (Camus (1971); Field, Dear, and Ogren (1989)) and numerical analysis (Haller, Ventikos,

Poulikakos, and Monkewitz (2002)).

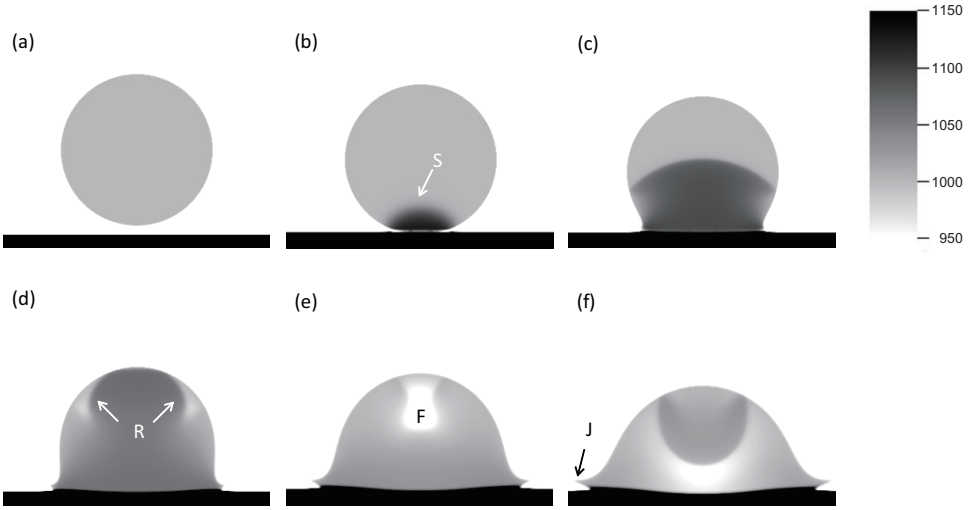

Figure 5: The density contours for droplet impact with a solid wall. The impact Mach number is 0.2, the target compliance is 0.04. The labels indicate S: Shock Wave, R: Reflected, F: Focus and J: Jetting

As mentioned before, in the initial stage of a droplet impact the non uniform pressure distribution which is greater than the water hammer pressure is generated. The generated pressures of two-dimensional and axisymmetric cases are plotted in Fig. 6 together with one-dimensional results. The pressure in the compressed area (Fig. 5 (b)) is initially constant, however the center pressure gradually decreases. On the other hand the edge pressure gradually increases until jetting occurs. In the Fig. 6 both the pressure for droplet center and the maximum pressure that occurs at the edge are shown. The detail of the pressure difference at low M_i cases are shown in Fig. 7. From Fig. 6 and Fig. 7, it is found that the generated pressure depends on the droplet impact Mach number M_i. For the high M_i case, the center pressure is almost same as 1D pressure and the edge pressure is about 3 times greater than the center pressure. This tendency reasonably agree with theories of Heymann (1969) and Lesser (1981) . They also described that the edge pressure is identical for 2D and 3D, but our results show that the 2D pressure is greater than the 3D pressure. From Fig. 7 as M_i decreases the edge pressure approaches the center pressure. These pressure are almost identical at the $M_i = 0.1$. It is also found that the center pressure decreases as the dimension increases and the center pressure of axi-symmetric case is almost half of the 1D pressure in a range of low M_i. This agrees with Engel's result Eq. (3).

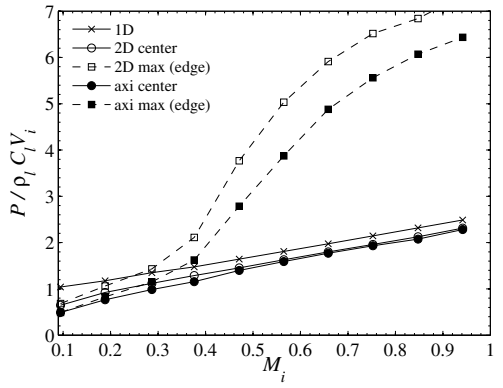

Figure 6: Comparison of generated pressure due to droplet impact

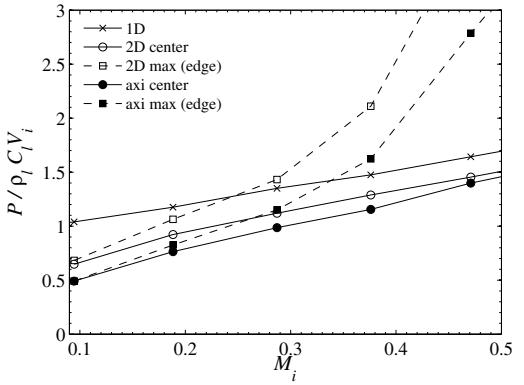

Figure 7: Close up figure for Fig. 6

Finally the effect of target compliance on the generated pressure is discussed. Fig. 8 shows the time history of the surface pressure with $\bar{Y} = 0.04$ and $\bar{Y} = 0.26$. The impact Mach number M_i is 0.5. This figure clearly shows that the generated pressure decreases as the target becomes more compressible or deformable. Especially the edge pressure is dramatically decreased. Fig. 9 shows differences in the target deformation between $\bar{Y} = 0.04$ and $\bar{Y} = 0.26$. This indicates that the wall deformation strongly depends on the target compliance, and the droplet dynamics and the generated pressure can change accordingly as observed in the present computations.

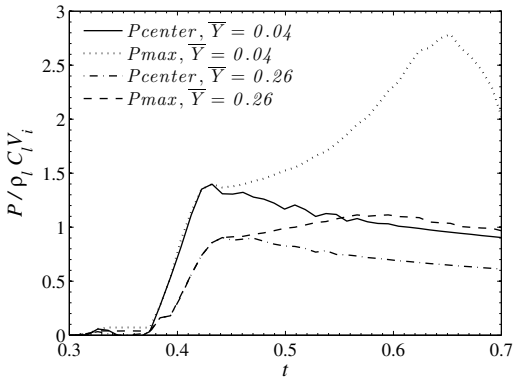

Figure 8: Time evolution of generated pressure ($M_i = 0.5$)

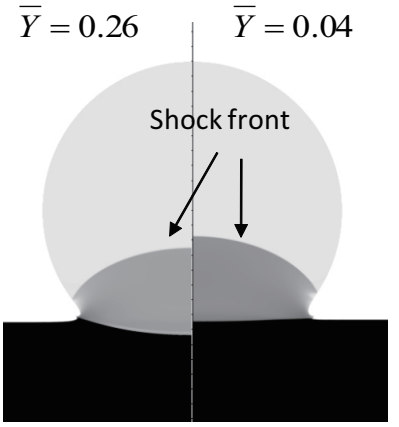

Figure 9: Target deformation due to the droplet impact ($M_i = 0.5$). Left and right show the case of $\bar{Y}$ of 0.04 and $\bar{Y}$ of 0.26, respectively

4 Conclusions

We numerically investigate a high speed droplet impact on a solid wall. The multi-component Euler equations with the stiffened equation of state are computed by a FV-WENO scheme with an HLLC Riemann solver that accurately captures shocks and interfaces. In order to compare the available theory and experiments, 1D, 2D and axi-symmetric solutions are obtained. It is found that the generated pressure depends on the droplet impact Mach number M_i. For the low M_i case the pressure differences at the center and the edge are minimized and the pressure is almost half

of the 1D case. On the other hand, for the high M_i case the edge pressure is almost 3 times greater than the center pressure. However, increasing the target compliance the edge pressure dramatically decreased.

Acknowledgement: This work was conducted during one of the author T. Sanada stayed at California Institute of Technology. T. S. appreciates the support by Murakawa Niro Foundation and Faculty of Engineering, Shizuoka University.

References

Brunton, J. H. (1966): High speed liquid impact. *Proc. R. Soc. London. Ser. A*, vol. 260, pp. 79–85.

Brunton, J. H.; Rochester, M. C. (1979): *Treatise on Materials science and technology, Erosion, Erosion of Solid Surface by the Impact of Liquid Drops*. Academic press.

Camus, J. J. (1971): *A study of high-speed liquid flow in impact and its effect on solid surface*. Ph.D. thesis, University of Cambridge.

Chen, H.; Liang, S. M. (2008): Flow visualization of shock/water column interactions. *Shock Waves*, vol. 17, pp. 309–321.

Cook, S. S. (1928): Erosion by water-hammer. *Proc. R. Soc. London. Ser. A*, vol. 119, pp. 481–488.

Field, J. E.; Dear, J. P.; Ogren, J. E. (1989): The effects of target compliance on liquid drop impact. *J. Appl. Phys.*, vol. 65, pp. 533–540.

Field, J. E.; Lesser, M. B.; Dear, J. P. (1985): Studies of two-dimensional liquid-wedge impact and their relevance to liquid-drop impact problems. *Proc. R. Soc. London. Ser. A*, vol. 401, pp. 225–249.

Gottlieb, S.; Shu, C. W. (1998): Total variation diminishing runge-kutta schemes. *Math. Comp.*, vol. 67, pp. 73–85.

Haller, K. K.; Ventikos, Y.; Poulikakos, D.; Monkewitz, P. (2002): Computational study of high-speed liquid droplet impact. *J. Appl. Phys.*, vol. 92, pp. 2821–2828.

Harlow, F.; Amsden, A. (1971): *Fluid Dynamics, Monograph LA-4700*. Los Alamos National Laboratory.

Heymann, F. J. (1968): On the shock wave velocity and impact pressure in high-speed liquid-solid impact. *J. Basic Engr. D*, vol. 90, pp. 400–402.

Heymann, F. J. (1969): High-speed impact between liquid drop and solid surface. *J. Appl. Phys.*, vol. 40, pp. 5113–5122.

Huang, Y. C.; Hammitt, F. G.; Mitchell, T. M. (1973): Note on shock-wave velocity in high-speed liquid-solid impact. *J. Appl. Phys.*, vol. 44, pp. 1868–1869.

Igra, D.; Takayama, K. (1999): Investigation of aerodynamic breakup of a cylindrical water droplet. *Report of the Institute of Fluid Science, Tohoku University*, vol. 11, pp. 123–134.

Igra, D.; Takayama, K. (2001): Numerical simulation of shock wave interaction with a water column. *Shock Waves*, vol. 11, pp. 219–228.

Johnsen, E.; Colonius, T. (2006): Implementation of weno schemes for compressible multicomponent flow problems. *J. Comput. Phys.*, vol. 219, pp. 715–732.

Johnsen, E.; Colonius, T. (2009): Numerical simulations of non-spherical bubble collapse. *J. Fluid Mech.*, vol. 629, pp. 231–262.

Lesser, M. B. (1981): Analytic solutions of liquid-drop impact problems. *Proc. R. Soc. London. Ser. A*, vol. 377, pp. 289–308.

Lesser, M. B.; Field, J. E. (1983): The impact of compressible liquids. *Ann. Rev. Fluid Mech.*, vol. 15, pp. 97–122.

Rochester, M. C.; Brunton, J. H. (1979): Pressure distribution during drop impact. *Proc. 5th Int. Conf. on Erosion by Solid and Liquid Impact*, pp. 6–1 – 6–7.

Saurel, R.; Abgrall, R. (1999): A multiphase godunov method for compressible multifluid and multiphase flows. *J. Comput. Phys.*, vol. 150, pp. 427–467.

Shu, S. W.; Osher, S. (1988): Efficient implementation of essentially non-oscillatory shock-capturing scheme. *J. Comput. Phys.*, vol. 77, pp. 439–471.

Thompson, P. A. (1988): *Compressible-Fluid Dynamics*. McGRAW-HILL.